Journal of Materials Chemistry C

ROYAL SOCIETY OF CHEMISTRY

PAPER

View Article Online
View Journal | View Issue

Cite this: *J. Mater. Chem. C*, 2025, **13**, 19244

Magnetic assembly approach to hierarchical photonic stripes

Jordan Austin-Frank Wilson, Allen Sun and Zhiwei Li *

Received 30th June 2025,
Accepted 14th August 2025

DOI: 10.1039/d5tc02507a

rsc.li/materials-c

Magnetic north and south poles attract, leading to the well-known end-on attachment between two magnets. In this work, we leverage distinct size-dependent dipole–dipole interactions between nanorod magnets-magnetized nanorods-to assemble hierarchical photonic stripes and provide an effective mechanism to prepare complex photonic materials with precisely tunable structural colours. Under a magnetic field, Fe_3O_4@SiO_2 nanorods are magnetized with an induced parallel magnetic dipole, favour a size-dependent equilibrium bonding state, and then assemble along a critical angle into an offset packing instead of the end-on attachments. Our experimental results and computational model indicate that magnetic nanorods exhibit a distinct bonding mode compared to magnetic nanospheres, underpinning the important role of magnetic anisotropy in determining the nanoscale magnetic interactions, structural symmetry, and photonic properties. This scale-dependent interaction produces tetragonal photonic crystals, which further assemble into hierarchical photonic stripes driven by magnetic repulsion between crystals at a high concentration under the assistance of a template. This work provides an assembly approach to fabricating photonic materials and devices that have orders across different length scales based on unique interactions between nanostructured materials.

Introduction

Photonic crystals are periodic structures that can display structural colours due to the constructive interference between light and the periodic arrangement of materials.[1–3] As described by Braggs' law, photonic crystals have demonstrated unique optical properties and have been broadly used for wave guide, optical sensing, anticounterfeiting, information encryption, and many other smart detections.[4–8] Their capability in manipulating photons through photonic bandgap engineering allows scientists to design photonic chips for optical communication, computing, and quantum information science.[9–11] Among many established methods, assembly of nanoparticles with defined sizes and shapes have demonstrated many advantages over lithography or fabrication methods, including high control over the crystal structures, precisely tunable structural colours, and dynamic optical responses to external stimuli.[2,12–14] To prepare the photonic crystals for practical applications, it is important to precisely control the interactions between nanoparticles because the strength and directionality of different types of interactions determine the photonic structures and optical properties of the crystals.[13] On the other hand, developing responsive photonic materials that show fast colour switching under external stimuli will benefit from exploring nanoscale interactions and precise control over the interaction's dynamics. To this end, understanding the interactions between nanoscale building blocks is a good starting point to identify proper forces to drive the assembly of photonic crystals.

Among various physical interactions, capillary force is one of the most broadly used physical interactions to assemble nanoparticles into photonic crystals.[15–17] During this physical process, the nanoparticle building blocks are first dispersed into a

Department of Chemistry and Biochemistry, University of Maryland, College Park, Maryland 20742, USA. E-mail: zlinano1@umd.edu

Zhiwei Li

Dr Zhiwei Li is an assistant professor in the Department of Chemistry and Biochemistry at the University of Maryland, College Park. He received his PhD in chemistry from the University of California, Riverside in 2019. He was a Richard P. Van Duyne postdoctoral fellow in the Department of Chemistry and the International Institute for Nanotechnology (IIN) at Northwestern University. His current research is focused on chemical synthesis and assembly of nanostructured materials for nanophotonics and quantum physics.

good solvent and then assembled on pre-designed substrates through solvent evaporation.[18–20] The strong capillary force assembles the nanoparticles into close-packed photonic crystals.[8,12,21] Because of the strong connection between the packed nanoparticles, it is practically difficult to dynamically tune the crystal periodicity and structural colours on the substrates. Therefore, exploring new driving forces that allow one to actively tune the connection between the building blocks is important to extend the applications of photonic crystals.[13] Instead of the evaporation-assembly approach to solid-state materials, magnetic assembly was developed to assemble magnetic nanoparticles into ordered structures in a solution phase.[22–27] The dipole–dipole coupling between neighbouring magnetic nanoparticles drives the assembly of two-dimensional or three-dimensional photonic crystals with vivid structural colours in a colloidal solution.[22,23,28–32] Because the strength of the induced dipoles of individual nanoparticles and the dipolar coupling between them is dependent on the strength of the external magnetic field, it is possible to tune the particle interactions and therefore the structural periodicity by simply changing the strength or direction of the external fields.[32–36] Therefore, magnetic assembly has been developed as a dynamic approach to responsive photonic crystals that show reversible colour switching in response to external stimuli.[1,36,37] For example, different types of nanoparticles, including nanospheres, nanocubes, and nanorods, have been assembled into responsive photonic crystals in solutions, which exhibit precisely controlled structural colours in response to either magnetic field strength or direction changes.[26,27,30,38,39] However, further processing these photonic materials into devices needs additional mechanisms to pattern the crystal materials into macroscale periodic structures that have order and complexity in different length scales. Here, we report direct magnetic assembly of Fe_3O_4@SiO_2 nanorods into hierarchical photonic crystals with orders across nano to macroscale and develop a reliable approach to photonic patterns with dynamic colour switching in response to a magnetic field. We studied the shape anisotropy of magnetic nanoparticles by using nanospheres and nanorods as model systems and discussed how the nanorod shape leads to a size-dependent bonding angle between two interacting nanorods as well as the formation of tetragonal photonic crystals in a magnetic field. This work elucidates new insights into the interaction dynamics between nanoparticles and provides a reliable approach to complex and responsive photonic patterns that can be used in device fabrication, sensing, anticounterfeiting, and information encryption.

Results and discussion

The magnetic assembly was performed in a solution of Fe_3O_4@SiO_2 nanorods under the presence of a permanent magnet. Fig. 1 illustrates the assembly process and working mechanism of the magnetic assembly of the hierarchical photonic stripes. Fe_3O_4@SiO_2 nanorods were used as building blocks and prepared based on a solid-state reduction method.[27,40,41]

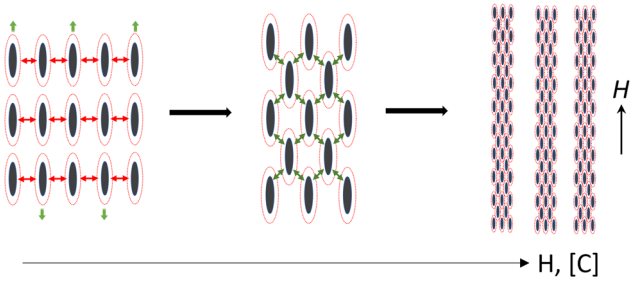

Fig. 1 Schematic illustration of the formation of hierarchical tetragonal photonic crystals. Under the application of a uniform magnetic field, the Fe_3O_4@SiO_2 nanorods are magnetized with an induced magnetic dipole parallel to the external field. Driven by the dipole–dipole attractions, the nanorods assemble into tetragonal photonic crystals along a critical angle that depends on the nanorods' separation and sizes. In a strong magnetic field and a high nanorod concentration, the crystals further pack into hierarchical photonic stripes with orders across different length scales under the assistance of a template.

Specifically, FeOOH nanorods (Fig. 2a) were synthesized in a room-temperature hydrolysis reaction of $FeCl_3$. A typical TEM image in Fig. 2a shows the uniform size, with a length of 322 ± 16 nm and width of 70 ± 5 nm based on the measurement of 50 nanorods in TEM images. SiO_2 shells of 50 nm were coated to form FeOOH@SiO_2 nanorods, which were further reduced to Fe_3O_4@SiO_2 nanorods (Fig. 2b) using a solid-state reduction process. When a magnetic field is applied to an aqueous dispersion of the magnetic rods, there is magnetic repulsion if the magnetic nanorods are side-by-side and magnetic attraction when they are aligned in a chain. Previous studies on magnetic assembly of nanospheres have shown that Fe_3O_4 nanospheres assemble into linear chains through an end-on attachment.[23,42,43] Consider that the Fe_3O_4@SiO_2 nanorods are magnetized with an induced magnetic dipole and imagine they behaviour like a nanoscale magnet. In a magnetic field, they are also expected to assemble through the end-on attachment

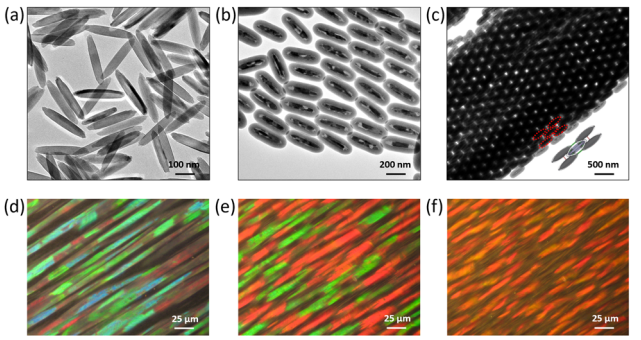

Fig. 2 Magnetic assembly of nanorods into tetragonal photonic crystals. TEM images of (a) FeOOH nanorods, (b) Fe_3O_4@SiO_2 nanorods, and (c) the tetragonal photonic crystals. Inset in (c) shows one unit cell of the body-centered tetragonal crystals. Nanorods in one unit cell are highlighted in dashed red ellipses. Optical microscopy images of the responsive photonic crystals under different magnetic field directions: (d) 0°, (e) 30°, and (f) 50°. The external magnetic field directions are defined by the angle between the field direction and the horizons in the incident planes as illustrated in Fig. S2d.

based on our understanding on how bulk magnets assemble. However, our studies show that there exists a thermodynamic bonding angle between magnetic nanorods, which define the equilibrium positions and are dependent on the nanorod sizes and separation. This thermodynamic bonding angle is a critical angle between the line vertical to the field direction and the line connecting two nanorods at the final equilibrium state, which is introduced to elucidate how the nanorods' interacts lead to size-dependent offset packing instead of the well-known end-on assembly in macroscopic magnets. These unique magnetic interactions between nanorods lead to the formation of a centred rectangular phase as shown in the middle scheme of Fig. 1. Within the assembled structures, the neighbouring nanorods assemble along the predicted thermodynamic critical angle. Such phases also grow out of the plane, leading to the formation of tetragonal photonic crystals. If a strong magnetic field is applied to a concentrated solution of the Fe_3O_4@SiO_2 nanorods, we propose the formation of hierarchical photonic stripes, with regular spacing and unidirectional alignment (the right scheme in Fig. 1). In the regime of high nanorod concentration and the strong field, the nanorods firstly assemble into tetragonal photonic crystals, and the formed crystals experience magnetic repulsion due to the parallel alignment to the external field and side-side configuration. This long-range magnetic repulsion drives the formation of regular, secondary photonic stripes in the concentrated solution.

The structure of the tetragonal photonic crystals is shown in the TEM image in Fig. 2c, which demonstrates high-quality periodicity and well-defined positional and orientational order of nanorods inside the single crystal. This TEM image is a projection of the single tetragonal crystal along its ⟨100⟩ crystal direction, leading to a centred rectangular phase. One unit cell is shown in Fig. 2c to illustrate the crystal orientation in the TEM image. The position of the nanorods is highlighted by red dots in Fig. S1a to elucidate the symmetry and positional order of the tetragonal photonic crystals. To analyse the unit cell, two parameters are introduced in Fig. S1, including *c* for periodicity along vertical direction and *a* for periodicity along other two directions. Based on the TEM image in Fig. S1b, we measured the pixel intensity of this image along the *a*- and *c*-axis, which is highlighted by green and red dashed lines in Fig. S1b. As demonstrated in Fig. S1c and d, unit cell parameter *c* is 476 ± 14 nm while a is 255 ± 23 nm, demonstrating high positional order and high-quality periodicity of the tetragonal photonic crystals. Under an optical microscope, a high-concentration solution of the magnetic nanorods does not show obvious structural colours (Fig. S2a). Under an external magnetic field, however, the magnetic nanorods assemble into tetragonal microcrystals and exhibit bright structural colours. In a horizontal magnetic field (0°), the crystals show green colours. When the field increases from the horizontal to vertical direction, the structural colours change from green to red under an optical microscope (Fig. 2d–f). Similarly, the photonic crystals have brilliant structural colours in a capillary and show colour changes from blue to red by changing the field directions (Fig. S2b) or viewing angles (Fig. S2c). This redshift of structural colours is due to the periodicity increases as the orientation changes of the microcrystals. Due to magnetic shape anisotropy, the nanorods and the anisotropic photonic crystals prefer to parallelly align their long axes to the external magnetic field directions, making it possible to dynamically tune the crystal orientation in solution phases. As a result, under a vertical incident light and a horizontal magnetic field (Fig. S1d), the diffraction occurs along the short axes of the nanorods, and the small periodicity produces green structural colours. When the magnetic field changes from horizontal to vertical directions, the periodicity will increase driven by the preferred alignment of crystals to the external magnetic field, leading to the redshift of the structural colours (Fig. S1d). The viewing angle-dependent structural colours can also be explained by the periodicity increases in Fig. S2e. When the viewing angle is zero, the diffraction occurs along the short axes of the nanorods, leading to green colour. Increasing the viewing angle to 60° leads to an increase in periodicity as well as the redshift of the observed colours.

To elucidate the formation mechanism of the tetragonal photonic crystals, we developed a three-dimensional model and computed the magnetic interactions between two nanorods using finite element analysis. Consider the shape anisotropy of the nanorods and image the magnetic interactions between the induced magnetic dipoles in each nanorod. It is difficult to calculate their magnetic interactions using the super magnetic dipole approximation, in which one assumes a magnetic dipole in the whole volume and neglects the shape effect of the nanorod. We consider the interactions between nanospheres and between nanorods in two models to elucidate how the shapes determine the interaction directionality and magnitudes. To do so, we use the finite element method and divide the magnetic nanospheres and nanorods into many, tiny volumes, with each volume having an induced magnetic dipole. The magnetic interactions are first calculated between any volume pairs of the two nanoparticles, and the force vectors are generated by summing over the whole nanoparticle volume to compute the overall magnetic interactions between the two nanoparticles. In Fig. 3a, we start with a two-nanosphere system and compute the magnetic force by changing one particle position from 0° to 90° under the presence of a horizontal magnetic field. The dependence of the magnetic interactions on the angles and the nanosphere separation is illustrated in Fig. 3b. Because the magnetic interaction between two dipoles is inversely proportional to the fourth power of their separation,[22,23] it is reasonable that the magnetic force magnitude decreases consistently as interparticle separation increases. The change in force direction is more important but difficult to analyse based on the force vector plots in Fig. 3b. We therefore decompose the magnetic forces into tangent and normal components in Fig. 3c and d, respectively. In the horizontal magnetic field, the tangent magnetic force first increases and then decreases as the angle changes from 0° to 90°. While there is a maximum magnitude, its direction is always pointing to the 90° position within the simulation domain, indicating that there is a consistent force to assemble

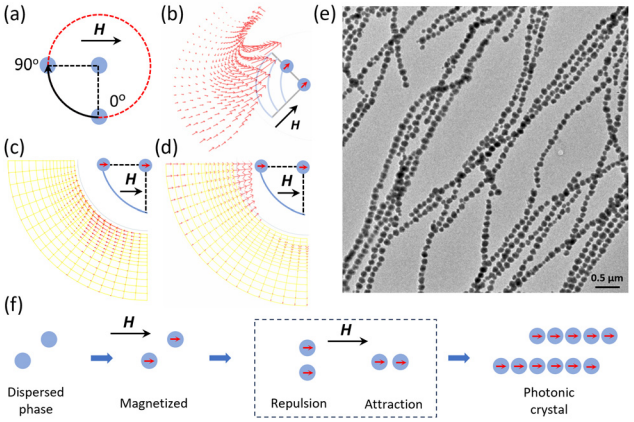

Fig. 3 (a) Schematic illustration of the magnetic interactions between two nanospheres. (b) Magnetic force mapping between the two nanospheres at different angles and separations. (c) The tangent and (d) normal components of the magnetic interactions at different angles. (e) The TEM image of the assembled one-dimensional chains under a magnetic field. (f) Schematic illustration of the magnetic interactions between nanospheres and the assembly into one-dimensional photonic crystals through the end-on attachment. The nanospheres are represented by blue dots. The external magnetic field and nanospheres' induced magnetic fields are indicated by black and red arrows, respectively.

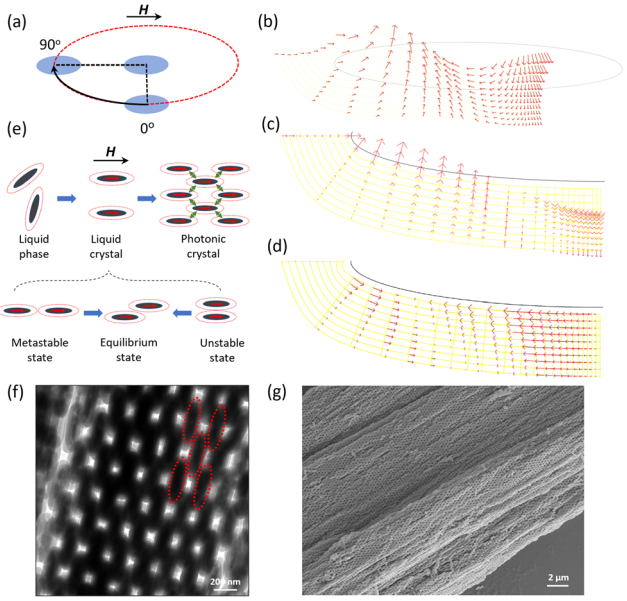

Fig. 4 Schematic illustration of the magnetic interactions between two nanorods. (a) Schematic illustration of the position change of one nanorod from 0° to 90° and their magnetic interactions are calculated at different angles and separations. (b) Magnetic force mapping between the two nanorods at different angles. (c) The normal and (d) tangent components (bottom) of the magnetic interactions at different angles. (e) Schematic illustration of the magnetic interactions between nanorods and the assembly into three-dimensional tetragonal photonic crystals along a critical angle. (f) TEM and (g) SEM images of the assembled tetragonal photonic crystals under a magnetic field.

the two nanospheres into linear chains along the 90° into an end-on configuration (Fig. 3c). We observed a simultaneous change in the normal component, whose interaction direction is highly dependent on the position of the nanospheres as defined by the angle. At 90°, there are strong attractions between the two nanospheres as the normal component is pointing to the primary nanosphere, leading to assembly of two nanospheres into the chains. At 0°, however, the normal component is pointing away, demonstrating a strong repulsion between the two nanospheres. This force analysis based on the finite element method predicts that the magnetic interaction between two identical nanospheres are directional, leading to repulsion and attraction domains depending on their separation, and that nanospheres assemble into linear chains along the direction of the external magnetic field. To experimentally verify this theoretical model, we used magnetic nanospheres as building blocks (Fig. S3) and assembled them by applying a magnetic field. As shown in the TEM image in Fig. 3e, we observed the formation of long chains made of the magnetic nanospheres. Therefore, this theoretical consideration is consistent with the long chains observed in TEM image as well as previous results on magnetic assembly of nanospheres into 1D chains.[23,43]

To study the magnetic interactions between magnetic nanorods, we used the same finite element analysis on two identical nanorods in a horizontal uniform magnetic field (Fig. 4a). The interparticle separation remains constant when the position of the secondary nanorod changes from 0° to 90°. The two magnetic nanorods are both horizontally oriented in the horizontal magnetic field due to the Zeeman coupling between the induced magnetic dipoles and the horizontal field.[26,44]

In an analogy to the case of the magnetic nanospheres, we divide the nanorod into tiny volumes and assume one induced magnetic dipole in each volume. Then, we compute the magnetic interactions between each volume pair in the two nanorods and sum over the volume pair interactions to calculate the overall magnetic forces. Fig. 4b shows the dependence of the magnetic interactions between the two nanorods on position and separation. We further plot the normal and tangent components of the magnetic interactions by mathematically decomposing the magnetic interactions. Based on the directionality of the normal force, we observed the presence of attraction and repulsion domains (Fig. 4c). Within the attraction domain, we noticed gradual decrease and then increase of the tangent component, demonstrating the presence of a critical point when the tangent component becomes zero (Fig. 4d). Further analysis on this critical point implies that there is no relative shift between the two nanorods and therefore defines a thermodynamic equilibrium state. At 90°, the tangent component also turns zero and the normal component demonstrates a strong attraction between the nanorods. However, a tiny thermal fluctuation would disassemble the nanorods from this position at 90° because, once the secondary nanorod is off this point driven by the fluctuation, the tangent force increases and is directing the nanorod away from the 90° position. One sequence of this event is the movement of the secondary nanorod to the position where the tangent force is zero within the attraction domain, which is driven by the normal force and leads to the equilibrium of the two nanorods at the critical angles. This theoretical analysis is important to identify the thermodynamics of the nanorod assembly,

demonstrating a quasi-stable state at 90° and the thermodynamic equilibrium state at the critical angle. More importantly, this model predicts that the magnetic nanorods prefer to assemble along a size-dependent critical angle. This new understanding explains the formation of the tetragonal photonic crystals (Fig. 4e). Due to the shape anisotropy of the nanorods, the resulting equilibrium status at the critical angle is different from our understanding of the bulky magnet interactions, which favour end-on assembly due to the north–south pole attraction. The packing of magnetic nanorods along the critical angles leads to the formation of the tetragonal photonic crystals. The predicted equilibrium state of the nanorods can be clearly verified by the positional orders in the TEM (Fig. 4f) and SEM (Fig. 4g) images. Considering the unit cell of the body-centered tetragonal crystal, we can experimentally determine the critical angle based on the unit cell parameters a and c (Fig. S4a). In the {100} plane, we measured the a and c to be 255 ± 23 nm and 476 ± 14 nm, respectively (Fig. S1). On the other hand, the critical angle is the angle (θ) between the line (blue arrow in the bottom left in Fig. S4a) connecting the two nanorods and the a-axis (green arrow in the bottom right in Fig. S4a) in the {110} plane. Overlapping multiple {100} and {110} planes produces different configurations, which can be used to identify the crystal orientation in TEM images. As a result, overlapping {110} and {100} planes lead to the formation of rectangular (Fig. S4b) and body-centered rectangular (Fig. S4c) phases, respectively. Based on this prediction, we could conclude that the projection image in Fig. S4d represents the multilayers of {100} planes, which is consistent with our understanding of Fig. 2c. Based on the geometry relation between the rod packing in the {100} and {110} planes, we find that there exists a geometry relation $\tan(\theta) = c/\sqrt{2}a$ and that θ is calculated to be 52.85° by using the unit cell parameters (a and c) measured from the TEM image in Fig. S4d and plotted in Fig. S1c and d. This experimental measurement can be verified by our theoretical model that is illustrated in Fig. 4. To do so, we considered different silica thickness from 5 nm to 50 nm and computed the tangent and normal magnetic forces between the magnetic nanorods. The results are plotted in Fig. S5a and b for the tangent and normal forces, respectively. Specifically, the zero points in the normal forces separate the repulsion domain from the attraction domain. When silica thickness increases from 5 nm to 50 nm, the angle where the normal magnetic force is zero decreases (Fig. S5b). By comparing the two plots, we can conclude that the critical angles are located within the attraction regime and that it is possible to predict the critical angles for nanorods of different silica thickness. In our experiments, the silica thickness was measured to be 50 nm. The critical angle when the tangent force is zero for 50-nm thick silica shells is shown to be 53.3° in Fig. S5a. This theoretically predicted angle by our analytical model is consistent with the experimentally calculated critical angle of 52.85° as derived from the TEM images and the periodicity plots in Fig. S1.

To observe the long-range order of the tetragonal photonic crystals, we could selectively etch away the Fe_3O_4 by HCl in the crystals, producing tetragonal crystals of the same structures made of hollow silica shells. A low-magnification TEM image of the SiO_2 nanoshells shows the long-range order of the tetragonal photonic crystals (Fig. S6). This observation combined with above structural analysis demonstrates the long-range order and high-quality periodicity of the formed photonic crystals. To further illustrate the positional order of the nanorods in the tetragonal crystals, two TEM images in Fig. S7a and b represent the projection of the (110) and (100) planes, respectively. Their relative crystal orientation can be explained by the crystal unit cell in the insets, which are consistent with the analysis presented in Fig. S4. Overall, our theoretical and experimental studies on magnetic interactions and assembly of nanorods provide new understanding of magnetic interactions between nanorods and new insights into the anisotropic interaction dynamics between anisotropic nanostructures, which further inspires the development of emerging photonic and electronic materials.

The presence of the size-dependent critical angles leads to the formation of offset packing of the nanorods into tetragonal crystals. Such periodic superstructures explain the observation of structural colours in an optical microscope (Fig. 1d–f). When prepared in a high concentration with the assistance of a template (Fig. S8), we observed well-defined hierarchical photonic stripes under the optical microscope (Fig. 5a). The photonic strips were aligned parallel to the external magnetic field and exhibit different colours if the field direction was changed. Such a simultaneous red shift of the structural colours is consistent with the increases in periodicity during the field direction changes. We then measured the reflection spectra of the photonic stripes during this process, and the strong diffraction peaks occur in the visible range due to the constructive interference of the light with the tetragonal crystals (Fig. 5b). As the field angle increases, the tetragonal photonic crystals rotate according to the external field. Under normal light incidence,

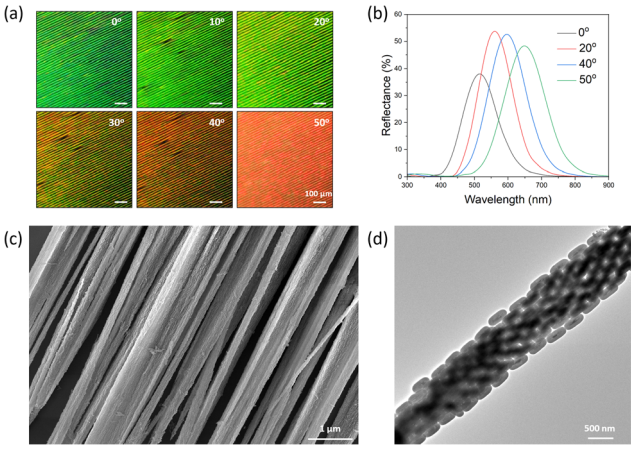

Fig. 5 Assembly of nanorods into hierarchical photonic structures in a strong magnetic field under the assistance of a template. (a) Optical microscopic images of the photonic structures under different field directions. (b) The reflection spectra of the photonic structures. (c) SEM and (d) TEM image of the photonic structures in a strong magnetic field.

the periodicity will increase, leading to the redshift of the structural colours. To verify the hierarchical photonic stripe structures and formation, the assembled photonic crystals were fixed by silica coating under the presence of the external magnetic field. While the nanorods were assembled into the hierarchical photonic stripes, the ongoing SiO_2 coating simultaneously occurred on the nanorod surface, which stabilized the hierarchical photonic stripes by forming a conformal coating. The SEM image in Fig. 5c indicates the strip-like morphologies of the assembled photonic crystals in the external magnetic field. Crystals have a very high aspect ratio in the magnetic field. Under high concentration and strong magnetic field, the nanorods first assembled in tetragonal photonic crystals with short fiber-like morphologies. Due to the parallel alignment of the fibers in the magnetic field, they experienced strong repulsion between their neighbouring fibers. One consequence of this event is the formation of longer photonic stripes through fusion of multiple fibers along the longitudinal direction, which is further regulated by the presence of the template. The strong repulsion along the transverse direction under the presence of the channel template produces the long-range periodic superstructures made of individual photonic stripe. The tetragonal packing of nanorods in the photonic stripes can be further verified in the TEM image in Fig. 5d, which confirms the formation of tetragonal photonic crystals and the long-range hierarchical photonic stripes in high concentration nanorod dispersion and a strong magnetic field.

Conclusions

We report the magnetic assembly of Fe_3O_4@SiO_2 nanorods into hierarchical tetragonal photonic stripes in a colloidal solution under the assistance of a template with pre-designed one-dimensional channels. Our experimental and simulation results demonstrate the presence of size-dependent critical angles between the Fe_3O_4@SiO_2 nanorods, which indicates the thermodynamic equilibrium bonding states between them in an external magnetic field. The resulting offset packing along the critical angle is different from the head-on attachment between magnetized bulky rod-shaped magnets and leads to the formation of tetragonal photonic crystals with anisotropic periodicity and well-defined porosity. This new understanding inspires the exploration of nanoscale interactions between nanostructured materials and their further assembly into hierarchical photonic structures with tunable physical properties. Based on the magnetic interactions between individual nanorods and between the photonic crystals, we observed the formation of hierarchical photonic stripes with highly tunable structural colours by simply changing the magnetic field directions under the presence of a template. This work provides an alternative assembly approach to complex photonic crystals with well-defined crystal structure anisotropy, as well as designer structural colours that can be remotely and reversibly controlled by external stimuli.

Experimental

Synthetic procedures

Preparation and assembly of Fe_3O_4@SiO_2 magnetic nanorods. The Fe_3O_4@SiO_2 magnetic nanorods were prepared by reducing FeOOH@SiO_2 nanorods in a tube furnace at 360 °C with forming gas (5% hydrogen and 95% nitrogen gas) as the reducing agent. The FeOOH nanorods were synthesized by hydrolysis of $FeCl_3$ (4 L, 0.04 M) at an ambient condition. After the hydrolysis reaction, the nanorods precipitated at the bottom of the reactors and were washed with Milli-Q water three times. The nanorod product was dispersed in 400-mL water as a stock solution for sequential PAA modification, silica coating, and high-temperature reduction. In the PAA modification process, 3 mL of FeOOH nanorods was added into 120-mL of PAA solution containing 43.2 mg of polyacrylic acid (PAA). The solution was stirred for 8 hours at ambient conditions. The products FeOOH–PAA were washed three times with Milli-Q water to remove excess amounts of PAA and dispersed in 9-mL water. In a typical silica coating process, 3-mL FeOOH–PAA nanorod dispersion was mixed with 1 mL of ammonia solution (28%) and 20 mL of ethanol. 100 μL of TEOS was added later in sequence to produce SiO_2 coating of 44 nm. The solution was washed with water three times and concentrated in 100 μL of water for high-temperature reduction. The Fe_3O_4@SiO_2 nanorods were prepared by reducing the FeOOH@SiO_2 nanorods in a solid state. The concentrated solution was transferred into a crucible and dried at ambient conditions. The powder was placed in a tubular furnace. The system was degassed with forming gas for 20 minutes and the temperature was raised to and kept at 360 °C for two hours. After reduction, the black powder was dispersed in water by sonication and washed three times against water. To improve the surface charge, the magnetic nanorods were modified by PAA (20 mL, 5 mg mL^{-1}) for 12 hours. The products were washed with water three times and dispersed in water for magnetic assembly. To characterize the crystal structures of the photonic crystals, we fixed them in 96-well plates by forming conformal silica coating. 25-μL Fe_3O_4@SiO_2 nanorod dispersion was transferred into the 96-well plate followed by adding 3 μL of ammonia, 100 μL of ethanol and 10 μL of TEOS. The plate was placed above a permanent magnet to assemble the nanorods into photonic crystals. After 10 minutes, 3 μL of ammonia was added to the solution, which enhanced the silica coating. After another 10 minutes, the precipitated photonic crystals were washed with water three times and were collected by magnetic separation. Sonication and centrifugation should be avoided because these treatments would break the crystal structures. The fixed photonic crystals were good for characterization in a solid state.

Polydimethylsiloxane (PDMS) templates were used to assemble the photonic stripes under the presence of a magnetic field. The structure of the templates is shown in Fig. S8. The PDMS films were prepared by mixing silicone elastomer base and curing agent at room temperature with a ratio of 10 : 1 (base to curing agent). The trapped bubbles during mixing were removed under vacuum for ~1 hour. The prepolymer solution

was then transferred to the surface of a commercial silicon wafer with stripe patterns in a Petri dish. Afterwards, the Petri dish was placed in an over at 80 °C for 2 hours to cure the PDMS template films. Through this soft lithography process, the PDMS templates can be prepared for assembly. To assemble the magnetic nanorods into photonic stripes, about 20 μL of the magnetic nanorods was added to the PDMS templates sitting on a glass subtract. A cover glass was placed on top of the liquid droplets. The sample was observed under an optical microscope while a magnetic field was applied to assemble the nanorods. The formed photonic stripes could be observed under the optical microscope.

Characterization

TEM images were taken on a JEM 2100 transmission electron microscope. SEM images were taken on a Hitachi SU-70 SEM. The reflection spectra were measured by the Ocean Optics HR4000 UV-NIR spectrometer. A magnetic field was applied to the solution of the magnetic nanorods at about 1 cm (~50 mT) to assemble and control the orientation of the photonic crystals.

Author contributions

The manuscript was written through contributions of all authors. All authors have approved the final version of the manuscript.

Conflicts of interest

There are no conflicts to declare.

Data availability

The data supporting the findings of this study is available within the article and its SI. Supplementary information: S1, crystal structure; S2, structural colors; S3, TEM images of Fe3O4 nanospheres; S4, crystal structure analysis of the photonic crystals; S5, magnetic interactions between two nanorods; S6, TEM image of colloidal crystals; S7, TEM images of crystals under different orientations; S8, SEM image of the templates. See DOI: **https://doi.org/10.1039/d5tc02507a**

Acknowledgements

This work was supported by the startup funds from the University of Maryland, College Park.

Notes and references

1 J. Ge and Y. Yin, *Angew. Chem., Int. Ed.*, 2011, **50**, 1492–1522.
2 Z. Cai, Z. Li, S. Ravaine, M. He, Y. Song, Y. Yin, H. Zheng, J. Teng and A. Zhang, *Chem. Soc. Rev.*, 2021, **50**, 5898–5951.
3 J. D. Joannopoulos, P. R. Villeneuve and S. Fan, *Solid State Commun.*, 1997, **102**, 165–173.
4 M. Butt, S. N. Khonina and N. Kazanskiy, *Opt. Laser Technol.*, 2021, **142**, 107265.
5 R. Zhang, Q. Wang and X. Zheng, *J. Mater. Chem. C*, 2018, **6**, 3182–3199.
6 P. Shen, Y. Zhang, Z. Cai, R. Liu, X. Xu, R. Li, J.-J. Wang and D. A. Yang, *J. Mater. Chem. C*, 2021, **9**, 5840–5857.
7 H. Xu, P. Wu, C. Zhu, A. Elbaz and Z. Z. Gu, *J. Mater. Chem. C*, 2013, **1**, 6087–6098.
8 J. Wang, P. W. Pinkse, L. I. Segerink and J. C. Eijkel, *ACS Nano*, 2021, **15**, 9299–9327.
9 M. Nakadai, T. Asano and S. Noda, *Nat. Photonics*, 2022, **16**, 113–118.
10 A. Kumar, M. Gupta, P. Pitchappa, N. Wang, P. Szriftgiser, G. Ducournau and R. Singh, *Nat. Commun.*, 2022, **13**, 5404.
11 M. Mandal, P. De, S. Lakshan, M. N. Sarfaraj, S. Hazra, A. Dey and S. Mukhopadhyay, *J. Opt.*, 2023, **52**, 603–611.
12 A.-Q. Xie, Q. Li, Y. Xi, L. Zhu and S. Chen, *Acc. Mater. Res.*, 2023, **4**, 403–415.
13 Z. Li, Q. Fan and Y. Yin, *Chem. Rev.*, 2021, **122**, 4976–5067.
14 G. von Freymann, V. Kitaev, B. V. Lotsch and G. A. Ozin, *Chem. Soc. Rev.*, 2013, **42**, 2528–2554.
15 Z. Zhou, Q. Li and X. Zhao, *Langmuir*, 2006, **22**, 3692–3697.
16 A. M. Brozell, M. A. Muha and A. N. Parikh, *Langmuir*, 2005, **21**, 11588–11591.
17 J. Hou, M. Li and Y. Song, *Angew. Chem., Int. Ed.*, 2018, **57**, 2544–2553.
18 M. B. Bigdeli and P. A. Tsai, *Langmuir*, 2020, **36**, 4835–4841.
19 M. Martusciello, C. Hervieu, D. Di Fonzo, A. Lanfranchi, P. Lova and D. Comoretto, *ACS Appl. Polym. Mater.*, 2025, **7**(8), 4779–4786.
20 C. Zhang, W. Li and Y. Wang, *J. Phys. Chem. Lett.*, 2022, **13**, 3776–3780.
21 E. Armstrong and C. O'Dwyer, *J. Mater. Chem. C*, 2015, **3**, 6109–6143.
22 Z. Li, F. Yang and Y. Yin, *Adv. Funct. Mater.*, 2020, **30**, 1903467.
23 L. He, M. Wang, J. Ge and Y. Yin, *Acc. Chem. Res.*, 2012, **45**, 1431–1440.
24 R. M. Erb, H. S. Son, B. Samanta, V. M. Rotello and B. B. Yellen, *Nature*, 2009, **457**, 999–1002.
25 S. Singamaneni, V. N. Bliznyuk, C. Binek and E. Y. Tsymbal, *J. Mater. Chem.*, 2011, **21**, 16819–16845.
26 Z. Li, M. Wang, X. Zhang, D. Wang, W. Xu and Y. Yin, *Nano Lett.*, 2019, **19**, 6673–6680.
27 Z. Li, C. Qian, W. Xu, C. Zhu and Y. Yin, *Sci. Adv.*, 2021, **7**, eabh1289.
28 Z. Fu, Y. Xiao, A. Feoktystov, V. Pipich, M.-S. Appavou, Y. Su, E. Feng, W. Jin and T. Brückel, *Nanoscale*, 2016, **8**(43), 18541–18550.
29 S. S. Park, Z. J. Urbach, C. A. Brisbois, K. A. Parker, B. E. Partridge, T. Oh, V. P. Dravid, M. Olvera de la Cruz and C. A. Mirkin, *Adv. Mater.*, 2020, **32**(4), 1906626.
30 Z. Li, X. Wang, L. Han, C. Zhu, H. Xin and Y. Yin, *Adv. Mater.*, 2022, **34**, 2107398.
31 Z. Li, Q. Fan, C. Wu, Y. Li, C. Cheng and Y. Yin, *Nano Lett.*, 2020, **20**, 8242–8249.

32 Z. Li and Y. Yin, *Adv. Mater.*, 2019, **31**, 1807061.
33 J. Ge and Y. Yin, *J. Mater. Chem.*, 2008, **18**, 5041–5045.
34 J. Ge and Y. Yin, *Adv. Mater.*, 2008, **20**, 3485–3491.
35 J. Ge, J. Goebl, L. He, Z. Lu and Y. Yin, *Adv. Mater.*, 2009, **21**, 4259–4264.
36 R. Xuan, Q. Wu, Y. Yin and J. Ge, *J. Mater. Chem.*, 2011, **21**, 3672–3676.
37 J. Ge, H. Lee, L. He, J. Kim, Z. Lu, H. Kim, J. Goebl, S. Kwon and Y. Yin, *J. Am. Chem. Soc.*, 2009, **131**, 15687–15694.
38 J. Ge, Y. Hu and Y. Yin, *Angew. Chem.*, 2007, **119**, 7572–7575.
39 M. Wang, L. He, W. Xu, X. Wang and Y. Yin, *Angew. Chem., Int. Ed.*, 2015, **54**, 7077–7081.
40 Z. Li, J. Jin, F. Yang, N. Song and Y. Yin, *Nat. Commun.*, 2020, **11**, 2883.
41 W. Xu, M. Wang, Z. Li, X. Wang, Y. Wang, M. Xing and Y. Yin, *Nano Lett.*, 2017, **17**, 2713–2718.
42 M. Wang, L. He, Y. Hu and Y. Yin, *J. Mater. Chem. C*, 2013, **1**, 6151–6156.
43 Y. Hu, L. He and Y. Yin, *Angew. Chem.*, 2011, **123**, 3831–3834.
44 Q. Fan, Z. Li, C. Wu and Y. Yin, *Precis. Chem.*, 2023, **1**, 272–298.